1 # Nighttime O(^{1}D) distributions in the mesopause region derived from
2 # SABER data

3 Mikhail Yu. Kulikov[1], and Mikhail V. Belikovich[1]
4 [1]Institute of Applied Physics of the Russian Academy of Sciences, 46 Ulyanov Str., 603950 Nizhny Novgorod, Russia

5 *Correspondence to*: Mikhail Yu. Kulikov (mikhail_kulikov@mail.ru)

6 **Abstract.** In this study, the new source of O(^{1}D) in the mesopause region due to the process OH($v{\geq}5$) + O(^{3}P) →

7 OH($0{\leq}v'{\leq}v{-}5$) + O(^{1}D) is applied to SABER data to estimate the nighttime O(^{1}D) distributions for the years 2003-2005. It is

8 found that O(^{1}D) evolutions in these years are very similar to each other. Depending on the month, monthly averaged O(^{1}D)

9 distributions demonstrate from 2 to 4 maxima with the values up to 340 cm^{-3} which are localized in height (at ~92-96 km)

10 and latitude (at ~20-40°S,N and ~60-80°S,N). Annually averaged distributions in 2003-2005 have a one weak maximum at

11 ~93 km and ~65°S with the values of 150-160 cm^{-3} and 3 pronounced maxima (with the values up to 230 cm^{-3}) at ~95 km

12 and ~35°S, at ~94 km and ~40°N, at ~93 km and ~65-75°N correspondingly. In general, there is slightly more O(^{1}D) in the

13 northern hemisphere than in the southern hemisphere. The obtained results are useful data set for subsequent estimation of

14 nighttime O(^{1}D) influence on chemistry of the mesopause region.

15 ## 1 Introduction

16 Daytime O(^{1}D) is considered to be one of the important chemical minor species of the stratosphere, mesosphere and

17 thermosphere, as it plays a significant role in the chemistry, and the radiative and thermal balance of this region (Brasseur &

18 Solomon, 2005). First of all, formed by photolysis of O_2 and O_3, O(^{1}D) is a mediator involved in the transformation of

19 absorbed solar radiation energy into the heating of this region and, in particular, excitation of $N_2(v)$ and $CO_2(v)$ (Harris &

20 Adams, 1983; Panka et al., 2017). Also, O(^{1}D) atoms participate in the reactions of destruction of long-lived greenhouse

21 gases (Baasandorj et al., 2012), CH_4 oxidation, and HO_x and NO_x production, for example:

22 O(^{1}D)+N_2O →2NO

23 O(^{1}D)+H_2O → 2OH

24 O(^{1}D)+H_2 → H+OH

25 O(^{1}D)+CH_4 → CH_3+OH

26 O(^{1}D)+CH_4 → H_2+CH_2O
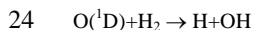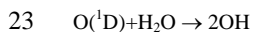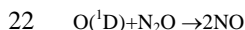
27 Moreover, the red line emission from O(^{1}D) atoms is one of the most important airglow phenomenon which are used as a

28 diagnostic of the ionosphere, for example, to monitor the electron density and neutral winds in the F region (Shepherd et al.,

29 2019). Therefore, many papers and experimental campaigns are devoted to measurements of features of O_3 photolysis to

30 O(^{1}D) (Taniguchi et al., 2003; Hofzumahaus et al., 2004).

31 Until recently, it was believed that the above mentioned processes stop at night as constant source of O(^{1}D) is absent while

32 the life time of the component is extremely low (less than 1 s). In principle, O(^{1}D) can be generated in sprite halos but for a

33 short duration of 1 ms (Hiraki et al., 2004). Recently, Sharma et al. (2015) and Kalogerakis et al. (2016) basing on laboratory

34 experiments proposed that O(^{1}D) could be produced in the mesopause region via process OH($v{\geq}5$) + O(^{3}P) → OH($0{\leq}v'{\leq}v{-}5$)

35 + O(^{1}D), that is multiquantum quenching of high excited states of OH by collisions with atomic oxygen in ground state.

36 Last year, Kalogerakis (2019) showed that a new model of O_2 A-band, that takes this process into account, describes well

37 (qualitatively and quantitatively) the results of early nighttime rocket measurements of volume emission rate profiles of this

38 airglow. Thus, he proved that the process OH($v{\geq}5$) + O(^{3}P) → OH($0{\leq}v'{\leq}v{-}5$) + O(^{1}D) really took place in nighttime

39 mesopause, and the produced O(^{1}D) distributions can be evaluated from available data.

40   In this study, the new source of O(^{1}D) in the mesopause region is applied to SABER data to estimate the O(^{1}D) nighttime

41   distributions for the years 2003-2005.

2 O(^{1}D) derivation from SABER Data

43   All processes used for O(^{1}D) determination are summarized in Table 1. Here, we apply the new OH(v) model of Fytterer et

44   al. (2019). Their "best-fit model" includes all commonly used production and loss processes of OH(v) (see Table 1), but

45   some parameters of the model, in particular, branching ratios of quenching OH(v)+O$_2$ and rate coefficients of OH($v \geq 5$) +

46   O(^{3}P) → OH($0 \leq v' \leq v$-5) + O(^{1}D) were adjusted with the use of volume emission rate profiles in four different wavelengths

47   measured by SABER and SCIAMACHY.

48   Due to low values of chemical lifetimes (less than 1 s), O(^{1}D) can be considered in chemical equilibrium:

49   $$O(^1D) = \frac{k_9 \cdot OH(9) \cdot O(^3P) + k_{10} \cdot OH(8) \cdot O(^3P) + k_{11} \cdot OH(7) \cdot O(^3P) + k_{12} \cdot OH(6) \cdot O(^3P) + k_{13} \cdot OH(5) \cdot O(^3P)}{k_{14} + k_{15} \cdot O_2 + k_{16} \cdot N_2}$$ (2)

50   Thus, to calculate local value of O(^{1}D) we should specify the local concentrations of OH(v=5-9) and O(^{3}P). The mentioned

51   model lets us to derive the OH(v) concentrations as the functions of the OH(v) source due to the reaction (1) ($P_{OH} = k_1 \cdot H \cdot$

52   O_3), air concentration (M), temperature (T), and O(^{3}P) concentration:

53   $$OH(v) = F_v(P_{OH}, M, T, O(^3P))$$ (3)

54   To determine O(^{3}P) and P_{OH}, we use known (e.g., Mlynczak et al., 2013, 2018) approach for O(^{3}P) derivation from the

55   simultaneous SABER measurements of volume emission rate of (9-7) and (8-6) OH transitions ($VER_{2\ \mu m}$), O$_3$ (9.6 μm), and

56   temperature (T). The approach employs the chemical equilibrium condition for nighttime ozone. As the result, it is done with

57   the use of the following system of equations:

58   $$\begin{cases} P_{OH} = k_2 \cdot O(^3P) \cdot O_2 \cdot M - k_3 \cdot O(^3P) \cdot O_3 \\ VER_{2\ \mu m} = k_4(9,7) \cdot F_9(P_{OH}, M, T, O(^3P)) + k_4(8,6) \cdot F_8(P_{OH}, M, T, O(^3P)) \end{cases}$$ (4)

59   Thus, we derive the local values of O(^{3}P), P_{OH}, and OH(v=5-9) from SABER data with the use of eqs. (3-4) and apply sets of

60   data (T, M, OH(v=5-9), and O(^{3}P)) to retrieve the local concentrations of O(^{1}D) with the use of eq. (2).

61

3 O(^{1}D) nighttime distributions

63   We use the version 2.0 of the SABER data product (Level2A) for the simultaneously measured $VER_{2\ \mu m}$, O$_3$, and T profiles

64   within the 0.01–0.0001 hPa pressure (p) interval (approximately 80–105 km in 2003-2005. We take only nighttime data

65   when the solar zenith angle χ > 95°. The range of latitudes covered by the satellite trajectory in a month was divided into 20

66   bins ~ (5.5-8)° each. 1500-3000 single profiles of O(^{1}D) concentration fall into one bin during a month of SABER

67   observations. For each bin we calculate monthly averaged zonal mean $< O(^1D) >$ distributions (hereafter, the angle brackets

68   are used to denote timely and spatially averaged values). For annually averaged distributions, we use 40 bins ~ 4° each.

69   Monthly averaged $< O(^1D) >$ distributions in corresponding month of 2003-2005 are shown in Figs. 1–3. Let's analyze the

70   presented data using the distributions in 2003 as an example. Depending on the range of latitudes covered by the satellite

71   trajectory in specified month, the figures show from 2 to 4 maxima which are localized in height (at ~92-96 km) and latitude

72   (at ~20-40°S,N and ~60-80°S,N). The values of the maxima can reach up to 300 cm^{-3} and more in both hemispheres and

73   different months, for example, in January-March and in May-August. Nevertheless, annual cycle of southern O(^{1}D)

74   demonstrates certain differences from northern one, i.e. many features of $< O(^1D) >$ in the southern hemisphere are not

75   repeated in the northern hemisphere with a shift of 6 months. In particular, the distributions in January-February show 2

76   pronounced maxima with close values (up to 300 cm^{-3}): the first one is at ~95 km and ~50-60°S, the second one is at ~93 km

77   and ~60-80°N. Half year later (in July-August), we can see 1-2 weak maxima in the southern hemisphere and a strongly

78   pronounced maximum at ~95 km and ~40-50°N. The similar pattern can be noticed comparing the $< O(^1D) >$) distributions

79   in June and December. The satellite trajectory in March and September allows us to observe simultaneously 4 maxima. Note

80   that the southern high-latitudinal maximum (up to 340 cm^{-3}) in March does not correspond to the relatively weak northern

81   high- latitudinal maximum in September.

82   The $< O(^1D) >$ evolutions in 2004-2005 are very similar to 2003. Nevertheless, one can see some differences. First of all, in

83   January-February 2004, there is pronounced particularity above 60°N below 90 km which does not appear in 2003 and 2005.

84   Kulikov et al. (2019) found the similar features in the latitude dependence of nighttime ozone chemical equilibrium

85   boundary in January–March 2004 above 60°N and connected it with abnormal dynamics of stratospheric polar vortex during

86   2003–2004 Arctic winter. There are additional features also which take place in a specific year, but absent in other two

87   years. In particular, the northern high-latitudinal maximum in January-February 2003 is remarkably higher (by the value)

88   than the ones in January-February 2004-2005. The southern high-latitudinal maximum (up to 340 cm^{-3}) in March 2003

89   corresponds to the same maximum in March 2005 but both maxima are remarkably higher than the one in March 2004. The

90   reverse (relative to December 2003 and 2005) ratio can be observed for the values of southern and northern maxima in

91   December 2004.

92   Annually averaged $< O(^1D) >$ distributions in 2003-2005 are shown in Fig. 4. There can be seen one weak maximum at

93   ~93 km and ~65°S with the values of 150-160 cm^{-3} and 3 pronounced maxima (with the values up to 230 cm^{-3}) at ~95 km

94   and ~35°S, at ~94 km and ~40°N, at ~93 km and ~65-75°N correspondingly. In general, there is slightly more O(¹D) in the

95   northern hemisphere than in the southern hemisphere.

96   The systematic uncertainty of presented data is defined mainly by uncertainties in $VER_{2\,\mu m}$, O$_3$, T measurements, and in the

97   rates of chemical and physical processes included in the OH(v) model. We repeated the analysis presented in Fytterer et al.

98   (2019) (see Sect. 3.4) and found that summarized uncertainty of O(¹D) varied in the range of (37-52)% depending on the

99   pressure level. Due to averaging, the random error of presented data is negligible.

100

101   **4 Discussion and Conclusion**

102   According to various early papers (Nicolet, 1959; Ghosh & Gupta, 1970; Shimazaki & Laird, 1970; Harris & Adams, 1983),

103   daytime O(¹D) concentrations at 90-100 km varied in the range of (10^2-10^3) cm^{-3}. Brasseur & Solomon (2005) published the

104   table (see Table A.6.2.c) where daytime O(¹D) changed from 70 cm^{-3} at 90 km to 140 cm^{-3} at 100 km. The presented results

105   show that monthly and annually mean nighttime O(¹D) concentrations at these altitudes can reach 300 cm^{-3} and 200 cm^{-3},

106   respectively. Thus, nighttime concentrations of O(¹D) are comparable with daytime concentrations of this component and, in

107   principle, can impact noticeably the chemistry and thermal balance of the mesopause region. More detailed analysis of this

108   impact should be carried out with the use of the global 3D chemical transport model of the mesosphere – lower

109   thermosphere.

110   **Data availability.** The SABER data used in this study can be downloaded from ftp://saber.gats-

111   inc.com/Version2_0/Level2A/. The presented data can be downloaded from

112   http://www.iapras.ru/english/structure/dep_240/dep_240.html.

113   **Author contributions.** Both authors contributed equally to this paper.

114   **Competing interests.** The authors declare that they have no conflict of interest.

115   **Acknowledgments.** The authors are grateful to the SABER team for data availability.

References

Adler-Golden, S.: Kinetic parameters for OH nightglow modeling consistent with recent laboratory measurements, J. Geophys. Res., 102, 19969–19976, doi:10.1029/97JA01622, 1997.

Baasandorj, M., Hall, B. D., and Burkholder, J. B.: Rate coefficients for the reaction of O(^{1}D) with the atmospherically long-lived greenhouse gases NF_3, SF_5CF_3, CHF_3, C_2F_6, c-C_4F_8, n-C_5F_{12}, and n-C_6F_{14}. Atmos. Chem. Phys., 12, 11753-11764, doi:10.5194/acp-12-11753-201, 2012.

Brasseur, G. P., and Solomon, S.: Aeronomy of the middle atmosphere: Chemistry and physics of the stratosphere and mesosphere (3rd ed). Dordrecht, Netherlands: Springer Science and Business Media, 2005.

Burkholder, J. B., Sander, S. P., Abbatt, J., Barker, J. R., Huie, R. E., Kolb, C. E., et al.: Chemical kinetics and photochemical data for use in atmospheric studies, evaluation no. 18, JPL Publication 15–10, Pasadena, CA: Jet Propulsion Laboratory, http://jpldataeval.jpl.nasa.gov, 2015.

Caridade, P. J. S. B., Horta, J.-Z. J., and Varandas, A. J. C.: Implications of the OCOH reaction in hydroxyl nightglow modeling, Atmos. Chem. Phys., 13, 1–13, doi:10.5194/acp-13-1-2013, 2013.

Fytterer, T., von Savigny, C., Mlynczak, M., and Sinnhuber, M.: Model results of OH airglow considering four different wavelength regions to derive night-time atomic oxygen and atomic hydrogen in the mesopause region, Atmos. Chem. Phys., 19, 1835–1851, doi:10.5194/acp-19-1835-2019, 2019.

Ghosh, S. N., and Gupta, S. K.: Altitude distributions of and radiations from certain oxygen and nitrogen metastable constituents, J. Geomagn. Geoelectr., 22, 329-339, 1970.

Harris, R. D., and Adams, G. W.: Where does the O(^{1}D) energy go? J. Geophys. Res., 88(A6), 4918–4928, doi:10.1029/JA088iA06p04918, 1983.

Hiraki, Y., Tong, L., Fukunishi, H., Nanbu, K., Kasai, Y., and Ichimura, A.: Generation of metastable oxygen atom O(^{1}D) in sprite halos, Geophys. Res. Lett., 31, L14105, doi:10.1029/2004GL020048, 2004.

Hofzumahaus, A., Lefer, B. L., Monks, P. S., Hall, S. R., Kylling, A., Mayer B. et al.: Photolysis frequency of O_3 to O(^{1}D): Measurements and modeling during the International Photolysis Frequency Measurement and Modeling Intercomparison (IPMMI), J. Geophys. Res., 109, D08S90, doi:10.1029/2003JD004333, 2004.

Hunt, B. G.: A diffusive-photochemical study of the mesosphere and lower thermosphere and the associated conservation mechanisms, J. Atm. Terr. Phys., 33, 1869-1892, 1971.

Kalogerakis, K. S., Smith, G. P., and Copeland, R. A.: Collisional removal of OH(X $^2\Pi$, v = 9) by O, O_2, O_3, N_2, and CO_2. J. Geophys. Res., 116, D20307, doi:10.1029/2011JD015734, 2011.

Kalogerakis, K. S., Matsiev, D., Sharma, R. D., and Wintersteiner, P. P.: Resolving the mesospheric nighttime 4.3 μm emission puzzle: Laboratory demonstration of new mechanism for OH(v) relaxation, Geophys. Res. Lett., 43, 8835–8843, doi:10.1002/2016GL069645, 2016.

Kalogerakis, K. S.: A previously unrecognized source of the O2 atmospheric band emission in earth's nightglow. Science Advances, 5, eaau9255, doi:10.1126/sciadv.aau9255, 2019.

Kulikov, M. Y., Belikovich, M. V., Grygalashvyly, M., Sonnemann, G. R., Ermakova, T. S., Nechaev, A. A., and Feigin, A. M.: Nighttime ozone chemical equilibrium in the mesopause region, J. Geophys. Res., 123, 3228–3242, doi:10.1002/2017JD026717, 2018.

Kulikov, M. Yu., Nechaev, A. A., Belikovich, M. V., Vorobeva, E. V., Grygalashvyly, M., Sonnemann, G. R., and Feigin, A. M.; Border of nighttime ozone chemical equilibrium in the mesopause region from saber data: implications for derivation of atomic oxygen and atomic hydrogen, Geophys. Res. Lett., 46, 997–1004, doi:10.1029/2018GL080364, 2019.

Mlynczak, M. G., Hunt, L. A., Mast, J. C., Marshall, B. T., Russell III, J. M., Smith, A. K., Siskind, D. E., Yee, J.-H., Mertens, C. J., Martin-Torres, F. J., Thompson, R. E., Drob, D. P., and Gordley, L. L.: Atomic oxygen in the mesosphere and

158   lower thermosphere derived from SABER: Algorithm theoretical basis and measurement uncertainty, J. Geophys. Res., 118,

159   5724–5735, doi:10.1002/jgrd.50401, 2013.

160   Mlynczak, M. G., Hunt, L. A., Russell, J. M., III, and Marshall, B. T.: Updated SABER night atomic oxygen and

161   implications for SABER ozone and atomic hydrogen, Geophys. Res. Lett., 45, 5735–5741, doi:10.1029/2018GL077377,

162   2018.

163   Nicolet, M.: The constitution and composition of the upper atmosphere, Proc. IRE, 47, 142-147, 1959.

164   Panka, P. A., Kutepov, A. A., Kalogerakis, K. S., Janches, D., Russell, J. M., Rezac, L., Feofilov, A. G., Mlynczak, M. G.,

165   and Yiğit, E.: Resolving the mesospheric nighttime 4.3 μm emission puzzle: Comparison of the $CO2(\nu_3)$ and $OH(\nu)$

166   emission models, Atm. Chem. Phys., 17, 9751–9760, doi:10.5194/acp-17-9751-2017, 2017.

167   Sharma, R. D., Wintersteiner, P. P., and Kalogerakis, K. S.: A new mechanism for OH vibrational relaxation leading to

168   enhanced CO_2 emissions in the nocturnal mesosphere, Geophys. Res. Lett., 42, 4639–4647, doi:10.1002/2015GL063724,

169   2015.

170   Shepherd, M., Shepherd, G., and Codrescu, M.: Perturbations of $O(^1D)$ VER, temperature, winds, atomic oxygen, and TEC

171   at high southern latitudes, J. Geophys. Res., 124, 4773–4795, doi:10.1029/2019JA026480, 2019.

172   Shimazaki, T., and Laird, A. R.: A model calculation of the diurnal variation in minor neutral constituents in the mesosphere

173   and lower thermosphere including transport effects, J. Geophys. Res., 75, 3221– 3235, doi:10.1029/JA075i016p03221, 1970.

174   Taniguchi, N., Hayashida, S., Takahashi, K., and Matsumi, Y.: Sensitivity studies of the recent new data on $O(^1D)$ quantum

175   yields in O_3 Hartley band photolysis in the stratosphere, Atmos. Chem. Phys., 3, 1293-1300, doi:10.5194/acp-3-1293-2003,

176   2003.

177   Varandas, A. J. C.: Reactive and non-reactive vibrational quenching in OCOH collisions, Chem. Phys. Lett., 396, 182–190,

178   doi:10.1016/j.cplett.2004.08.023, 2004.

179   Xu, J., Gao, H., Smith, A. K., and Zhu, Y.: Using TIMED/SABER nightglow observations to investigate hydroxyl emission

180   mechanisms in the mesopause region, J. Geophys. Res., 117, D02301, doi:10.1029/2011JD016342, 2012.

181

183   **Table 1. List of processes.**

184

		Process	Rate	Reference
	1	$H + O_3 \rightarrow O_2 + OH(v)$	$k_1, k_1(v)$	Burkholder et al. (2015), Alder-Golden (1997, Table 1)
	2	$O(^3P) + O_2 + M \rightarrow O_3 + M$	k_2	Burkholder et al. (2015)
	3	$O(^3P) + O_3 \rightarrow 2O_2$	k_3	Burkholder et al. (2015)
	4	$OH(v) \rightarrow OH(v')$	$k_4(v, v')$	Xu et al. (2012, Table A1)
	5	$OH(v) + N_2 \rightarrow OH(v') + N_2$	$k_5(v, v')$	Adler-Golden (1997, Table 1), Kalogerakis et al. (2011)
	6	$OH(v) + O_2 \rightarrow OH(v') + O_2$	$k_6(v, v')$	Adler-Golden (1997, Table 3), corrected and adjusted by Fytterer et al. (2019)
	7	$OH(v) + O(^3P) \rightarrow H + O_2$	$k_7(v)$	Varandas (2004, Table 3, M I)
	8	$OH(v) + O(^3P) \rightarrow OH(v') + O$	$k_8(v, v')$	Caridade et al. (2013, Table 1)
	9	$OH(9) + O(^3P) \rightarrow OH(3,4) + O(^1D))$	k_9	Fytterer et al. (2019)
	10	$OH(8) + O(^3P) \rightarrow OH(3) + O(^1D))$	k_{10}	Fytterer et al. (2019)
	11	$OH(7) + O(^3P) \rightarrow OH(\leq2) + O(^1D))$	k_{11}	Fytterer et al. (2019)
	12	$OH(6) + O(^3P) \rightarrow OH(\leq1) + O(^1D))$	k_{12}	Fytterer et al. (2019)
	13	$OH(5) + O(^3P) \rightarrow OH + O(^1D))$	k_{13}	Fytterer et al. (2019)
	14	radiative decay of $O(^1D)$	k_{14}	Burkholder et al. (2015)
	15	$O(^1D) + O_2 \rightarrow O(^3P) + O_2$	k_{15}	Burkholder et al. (2015)
	16	$O(^1D) + N_2 \rightarrow O + N_2$	k_{16}	Burkholder et al. (2015)

185

186

187 **Figures**

188
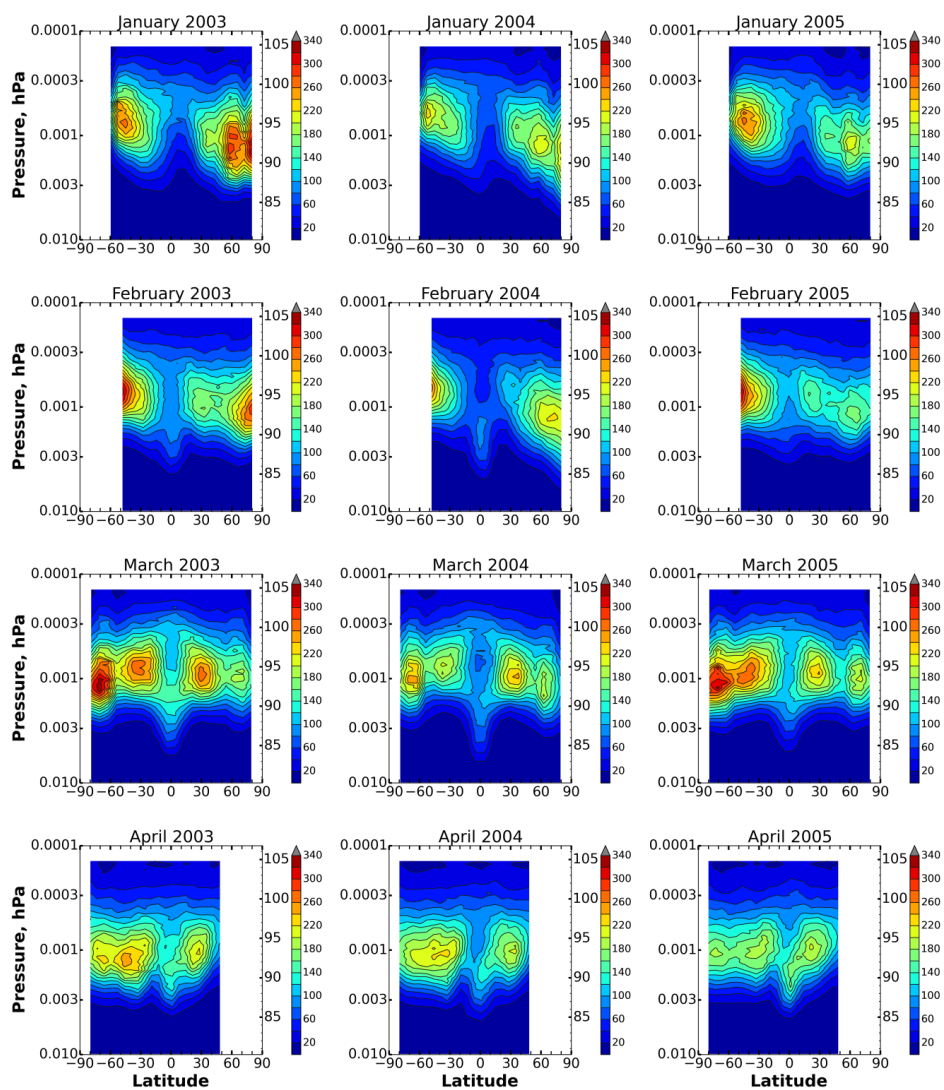
189

190

191   **Figure 1. Monthly averaged O(^{1}D) concentration (in cm^{-3}) in January-April of 2003-2005.**

192

193

194
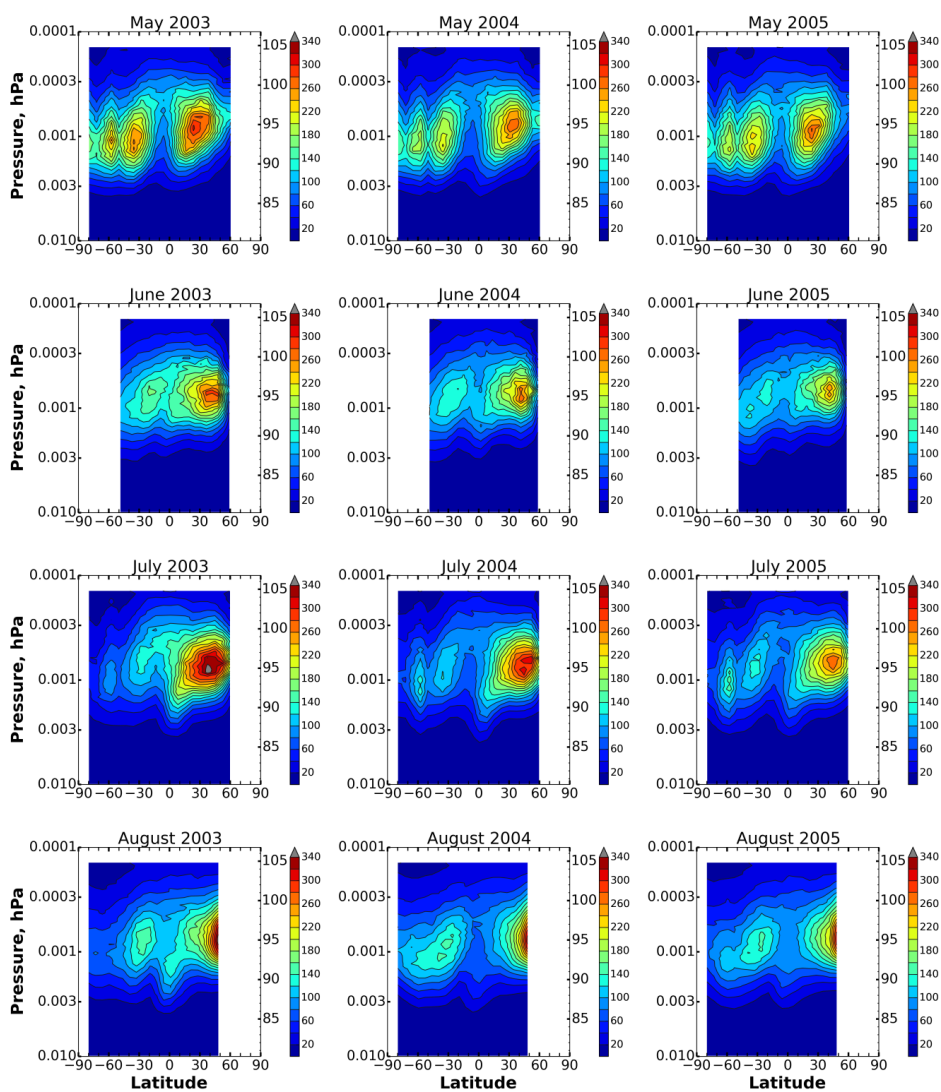
195

196   **Figure 2. Monthly averaged O(^{1}D) concentration (in cm^{-3}) in May-August of 2003-2005.**

197

198

199

200
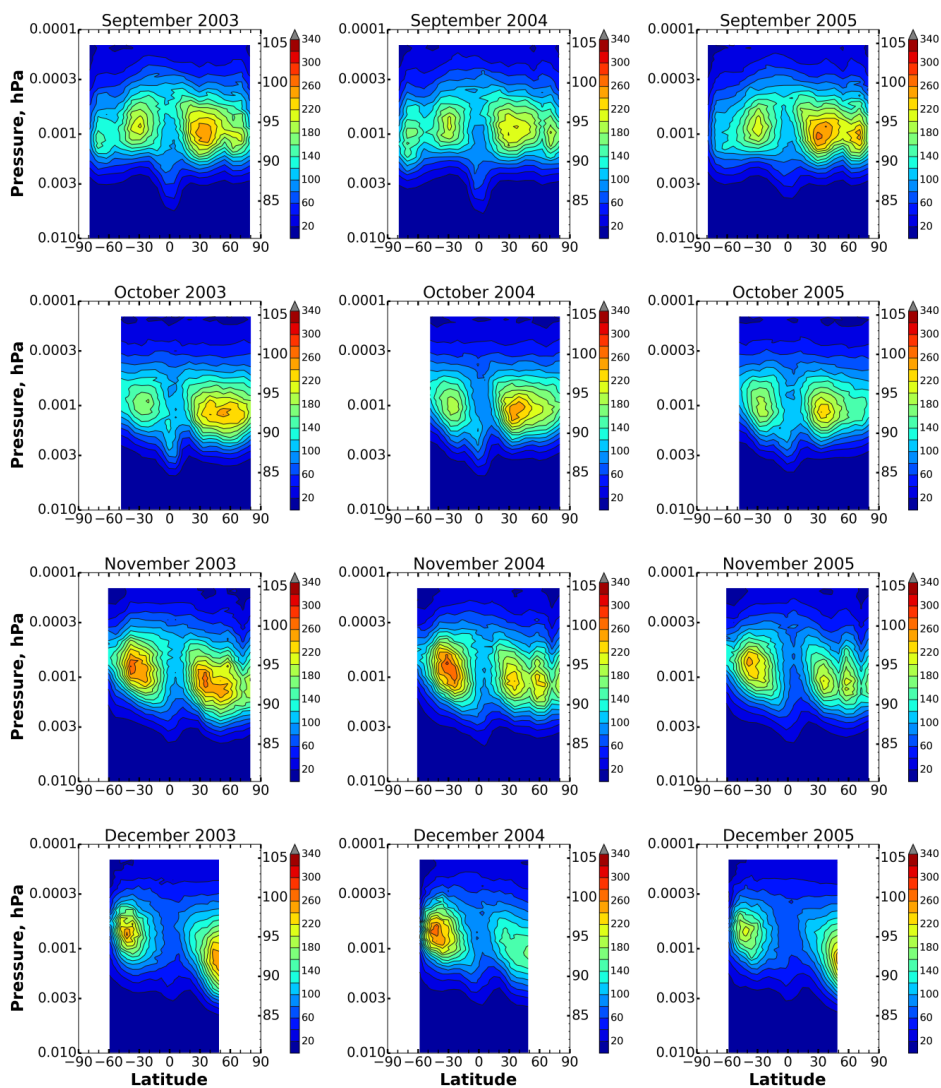
Figure 3. Monthly averaged O(^{1}D) concentration (in cm^{-3}) in September-December of 2003-2005.

202

203
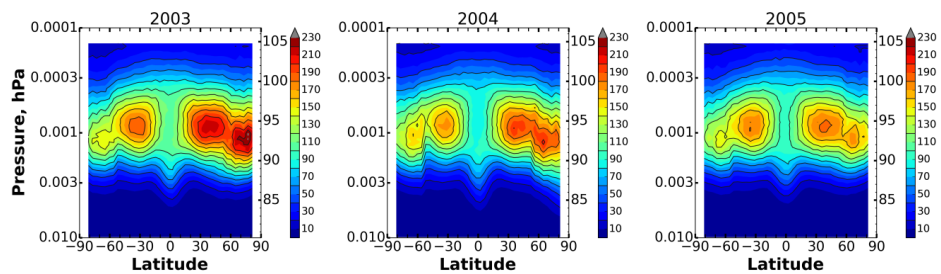
204

205   **Figure 4. Annually averaged O(^{1}D) concentration (in cm^{-3}) in 2003-2005.**